Chemical Science

ROYAL SOCIETY OF CHEMISTRY

EDGE ARTICLE

View Article Online
View Journal | View Issue

Cite this: *Chem. Sci.*, 2025, **16**, 19226

All publication charges for this article have been paid for by the Royal Society of Chemistry

Promoting selective electrochemical CO_2 reduction under unconventionally acidic conditions through secondary coordination sphere positioning

Kaeden Teindl, Jolene P. Reid and Eva M. Nichols *

While several studies have investigated the effects of protic secondary coordination sphere (SCS) groups on the kinetics of iron tetraphenylporphyrin (FeTPP) catalysed CO_2 reduction, few have examined how a protic SCS might alter reaction selectivity. Under mildly acidic conditions, FeTPP-based catalysts are selective towards the $2e^-/2H^+$ reduction of CO_2 to CO; however, in the presence of more acidic proton donors, indiscriminate proton transfers often result in parasitic H_2 evolution. This report investigates how SCS amide positioning alters CO *versus* H_2 selectivity during CO_2 reduction with a series of four FeTPP isomers bearing SCS amides at varying positions around the porphyrin core: NH donors are placed at either the *meta* or *ortho* position of the *meso* aryl porphyrin ring, as well as proximal (closer) or distal (farther away) to the porphyrin plane. In the presence of a conventional, weakly acidic proton source (phenol; $pK_a = 29.2$ in MeCN), all isomers display the expected high faradaic efficiency (FE) towards CO ($FE_{CO} = 67–85\%$) along with minimal H_2 evolution ($FE_{H_2} = 3–13\%$). With a significantly stronger acid (3,5-bis(trifluoromethyl)phenol; $pK_a = 23.8$ in MeCN), H_2 becomes the major product when using the *ortho*-distal or both *meta* isomers ($FE_{H_2} = 45–65\%$) as well as unfunctionalized FeTPP ($FE_{H_2} = 78\%$). Importantly, the *ortho*-proximal isomer shows dramatically rescued CO selectivity under these unconventionally acidic conditions ($FE_{CO} = 83 \pm 4\%$). These results show how proper SCS placement impacts reaction selectivity during CO_2 reduction, particularly with respect to minimizing indiscriminate proton transfers that lead to undesirable reactivity.

Received 26th June 2025
Accepted 7th September 2025

DOI: 10.1039/d5sc04700e

rsc.li/chemical-science

1. Introduction

Electrochemical CO_2 reduction offers a sustainable strategy to convert this inert molecule into value-added products, but significant kinetic barriers hinder efficient and selective CO_2 conversion.[1,2] While many transition metal electrocatalysts show promising reactivity,[3,4] efforts to improve their activity through primary coordination sphere modifications often follow electronic scaling relationships, wherein more negative reduction potentials are required to achieve faster catalytic turnover.[5,6] Taking inspiration from enzymes,[7–9] these scaling relationships may be 'broken' through modification of the secondary coordination sphere (SCS). The SCS consists of functional groups in the catalyst periphery that can modulate the kinetics and thermodynamics of individual reaction steps, or change the reaction mechanism altogether.[6,10–14]

During electrocatalytic CO_2 reduction, protic functional groups in the SCS may alter reaction barriers by stabilizing high-energy transition states and/or by relaying protons from an exogenous acid to bound substrate. Important contributions were made by Savéant and co-workers, who showed that modification of iron tetraphenylporphyrin (FeTPP) to include phenolic SCS donors substantially increases the kinetics of CO_2 reduction while maintaining high selectivity for CO.[15,16] Many subsequent investigations—including some from our laboratory—sought to understand how the kinetics of FeTPP-catalysed CO_2 reduction depend on protic SCS donor positioning,[17] proton transfer driving forces,[18–22] reactant templating,[23] and altering the number of protic groups in the SCS.[24–26]

Although the kinetic advantages of protic SCS groups have been frequently explored, very few studies have focused on how the SCS influences product selectivity during CO_2 reduction, especially with respect to SCS donor positioning. Typically, the selectivity of FeTPP catalysts is constrained to either the $2e^-/2H^+$ reduction of CO_2 to CO or—under sufficiently acidic conditions—the background reduction of protons to form H_2. However, recent reports have suggested that protic SCS groups may beneficially alter the selectivity of this platform. One notable example from Robert and co-workers describes the challenging $8e^-/8H^+$ reduction of CO_2 into CH_4 with a catalyst bearing pendent phenols, although this transformation was

Department of Chemistry, The University of British Columbia, Vancouver, British Columbia, V6T 1Z1, Canada. E-mail: enichols@chem.ubc.ca

driven photocatalytically.[27] The Dey group reported that iron porphyrinoid catalysts bearing protic SCS groups alter selectivity between CO and $HCOO^-$,[28] or enhance selectivity towards CO and against parasitic H_2 evolution.[29] Nevertheless, a full understanding of the numerous roles of the SCS is still emerging, and it remains unclear how an SCS group might be designed to achieve a desired selectivity change during FeTPP-catalysed CO_2 reduction.

When FeTPP catalysts are paired with highly acidic proton sources in solution, indiscriminate proton transfers often result in background H_2 evolution or catalyst degradation, rather than productive CO evolution.[30–32] For example, Costentin and Savéant reported that CO_2 reduction with [FeTPP]Cl using acetic acid (pK_a(DMSO) = 12.6,[33] pK_a(MeCN) = 23.5)[34] results in a FE_{CO} of only ~30%, along with formation of a green catalyst byproduct hypothesized to be a hydrogenated porphyrinoid.[30] To avoid low CO faradaic efficiencies and/or catalyst decomposition, FeTPP-catalysed CO_2 reduction typically employs mild Brønsted acids, such as phenol (pK_a(DMSO) = 18.0,[35] pK_a(MeCN) = 29.2);[34] however, this limits catalytic activity as FeTPP systems generally exhibit faster kinetics with stronger acids.[18,30] In order to maintain high CO selectivity under highly acidic conditions, it is crucial for protons to be directed to the bound CO_2 substrate rather than to the metal or porphyrin ligand. Whether and how a protic SCS regulates the desired proton transfers during CO_2 reduction remains poorly understood.

Against this backdrop, we sought to establish design principles for a protic SCS that can improve selectivity towards CO and against parasitic H_2 evolution. We hypothesized that indiscriminate proton transfers—and their deleterious effects on selectivity—could be minimized with an SCS donor that is suitably positioned near the catalytic active site. Accordingly, we designed a series of FeTPP complexes bearing pendent amides at varying positions around the catalytic active site to investigate the effects of SCS donor positioning on the selectivity and activity of FeTPP-catalysed CO_2 reduction (Scheme 1). We report the synthesis and electrochemical investigation of four positional isomers having NH donors at either the *meta* or *ortho* position of the *meso* aryl porphyrin ring, as well as either proximal (closer) or distal (farther away) to the porphyrin plane. The CO_2 reduction selectivity and activity of each isomer is reported in MeCN electrolyte in the presence of two different exogenous acids: phenol as a more conventional Brønsted acid (pK_a = 29.2 in MeCN), and 3,5-bis(trifluoromethyl) phenol as a stronger proton donor (pK_a = 23.8 in MeCN).[34] Using phenol as the exogenous acid, proper SCS donor positioning increases the CO_2 reduction rate constant by 10-fold while only modestly affecting CO *vs.* H_2 selectivity. However, in the presence of the more acidic proton source, we observe marked differences in reaction selectivity between each isomer: when the NH of the amide is positioned at the *ortho*-proximal position, CO is produced as the major product at a high faradaic efficiency (FE) of 83 ± 4% and only minor quantities of H_2 are formed (FE_{H_2} = 7 ± 1%), while each of the remaining isomers display a low FE for CO ($FE_{CO} \leq 27\%$) and significant background H_2 evolution ($FE_{H_2} \geq 45\%$). Together, these results provide insight into how suitable SCS donor positioning can regulate proton transfer to the active site and effect beneficial changes in reaction selectivity.

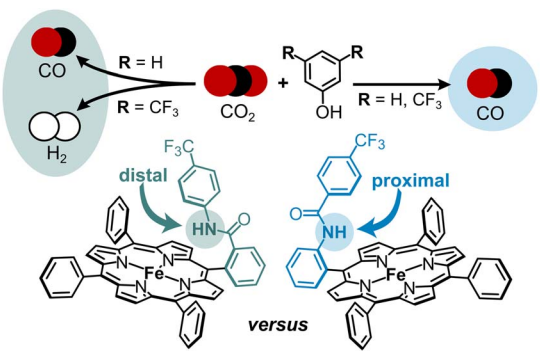

Scheme 1 *Ortho* distal *versus* proximal positioning of the SCS donor alters selectivity between CO and H_2 in the presence of a strong exogenous acid.

2. Results and discussion

2.1 Design and synthesis of four amide functionalized porphyrin isomers

Building on our previous work with FeTPP catalysts bearing tuneable SCS amides,[17,18] we envisioned a series of four structurally analogous positional isomers bearing amide pendants at varying positions around the iron porphyrin core: **Fe-*ortho*-proximal** features the amide pendant at the *ortho* position of the *meso* aryl ring with the NH proximal (closer) to the porphyrin plane, while **Fe-*ortho*-distal** places the NH distal (farther away) from the active site. The effects of the latter isomer on activity and selectivity are of particular interest since previous reports on protic SCS groups have largely focused on donors positioned at the *ortho*-proximal position for the sake of synthetic practicality.[15,18,24,36–39] We additionally prepared the two corresponding *meta* isomers (**Fe-*meta*-distal** and **Fe-*meta*-proximal**) to serve as control complexes. The *meta* isomers were selected as suitable controls over the *para*-substituted congeners because iron porphyrins functionalized with amide groups at the *para*-position of the *meso* porphyrin ring are known to display non-idealized behaviour under electrochemical conditions.[17,23]

The synthetic details of each iron porphyrin isomer are outlined in Scheme 2. **Fe-*ortho*-proximal** was prepared by the method we have previously reported:[18] first, 5-(*ortho*-nitrophenyl)-10,15,20(triphenyl) porphyrin, **1**-*ortho*, is reduced by $SnCl_2$ in concentrated HCl to afford 5-(*ortho*-aminophenyl)-10,15,20(triphenyl) porphyrin, **2**-*ortho*. Subsequent reaction of **2**-*ortho* with triethylamine and *in situ* generated 4-trifluormethyl benzoyl chloride provides the *ortho*-proximal amide porphyrin, **3**-*ortho*, which is metalated with $FeCl_2 \cdot 4H_2O$ to yield **Fe-*ortho*-proximal**. The corresponding *meta* isomer, **Fe-*meta*-proximal**, was synthesized according to the same procedure by using the *meta*-nitrophenyl porphyrin, **1**-*meta*, as starting material. To prepare the distal isomer, **Fe-*ortho*-distal**, 5-(methyl *ortho*-benzoate)-10,15,20(triphenyl) porphyrin, **4**-*ortho*, is first

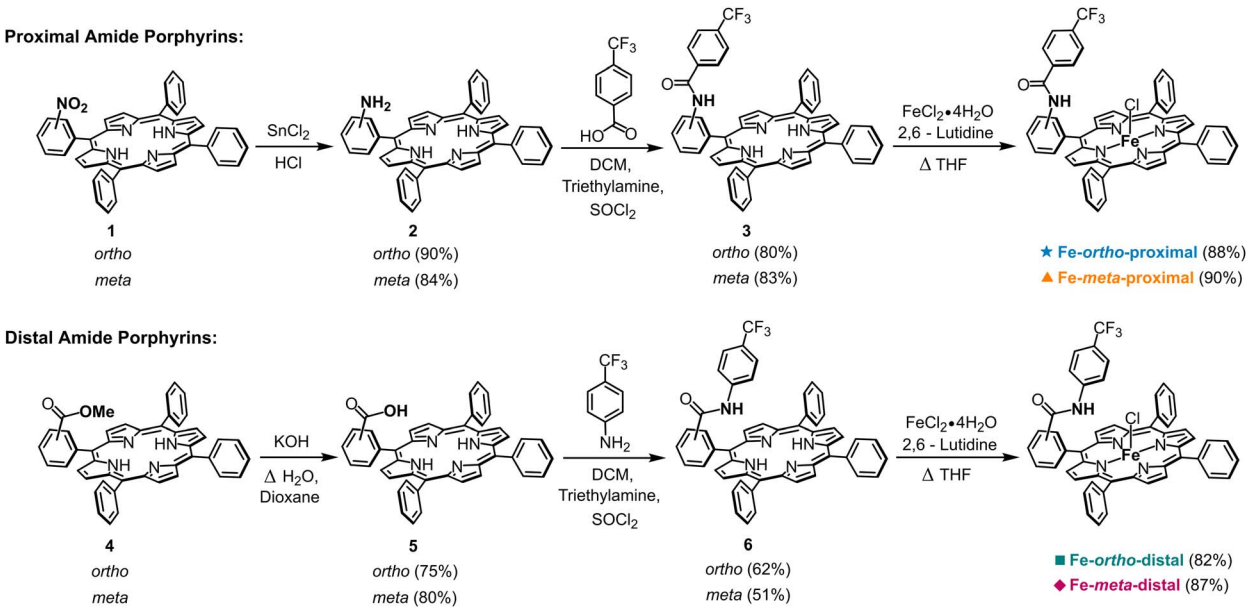

Scheme 2 Synthesis of each amide-functionalized porphyrin isomer. Top route is used to prepare Fe-*ortho*-proximal and Fe-*meta*-proximal, while bottom route is used to prepare Fe-*ortho*-distal and Fe-*meta*-distal.

hydrolysed in refluxing 1,4-dioxane and aqueous KOH to afford 5-(*ortho*-carboxyphenyl)-10,15,20(triphenyl) porphyrin, **5**-*ortho*. This intermediate is treated with $SOCl_2$ and triethylamine before the addition of 4-trifluoromethyl aniline to yield the *ortho*-distal amide functionalized porphyrin, **6**-*ortho*. Metalation of freebase **6**-*ortho* using $FeCl_2 \cdot 4H_2O$ provides **Fe-*ortho*-distal**. The corresponding *meta* isomer, **Fe-*meta*-distal**, was prepared identically by starting from the methyl *meta*-benzoate porphyrin, **4**-*meta*. All porphyrin ligands were fully characterized by ^1H, ^{19}F, and ^{13}C NMR spectroscopies. Each freebase and metalloporphyrin was additionally characterized by UV-vis spectroscopy and electrospray ionization mass spectrometry. Detailed synthetic procedures and characterization of all novel compounds can be found in the SI.

2.2 Computational and spectroscopic analysis of pendent amide conformation

First, computational analysis was performed on each isomer to predict the lowest energy conformation of each amide pendant. To streamline these calculations, the analogous closed-shell zinc porphyrins were analysed in favour of the open-shell iron complexes. We note that the conformation of the porphyrin scaffold is nearly identical when comparing iron and zinc porphyrins,[17,18,23] and metal identity is thus expected to have a minimal effect on pendent amide orientation. Conformational screening of each amide pendant was first performed using Macromodel and the lowest energy conformers were subsequently optimized using Density Functional Theory (DFT) (see Fig. S1 and the SI for details). The computed structure of each zinc complex is depicted in Fig. 1. Consistent with our previous reports,[17,18] the amide NH in **Zn-*ortho*-proximal** is positioned to facilitate intramolecular proton transfer and/or hydrogen bonding with a metal-bound CO_2 adduct. By contrast, in **Zn-*ortho*-distal** there is a notable interaction between the amide aryl ring and the porphyrin π system that leads the amide NH to point slightly away from the metal active site in the predicted lowest energy conformation. The pendent amides in the two *meta* isomers are positioned far from the active site and are therefore expected to exhibit minimal interactions with bound substrate, consistent with their role as positional controls.

We turned to NMR spectroscopy for experimental corroboration of these computational results. ^1H NMR spectra of the freebase porphyrins show that the chemical shift of the amide proton varies significantly with its positioning relative to the porphyrin ring: this peak appears at 9.82 ppm for the *ortho*-

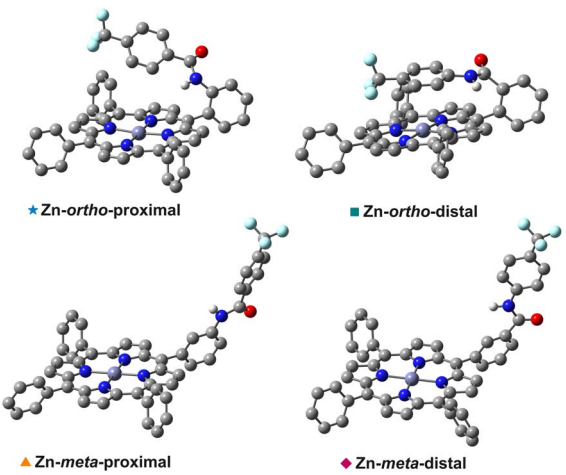

Fig. 1 Computed DFT structures of each Zn complex displaying the predicted lowest energy conformation of the amide pendant (see the SI for computational details).

proximal isomer and 11.04 ppm for the *ortho*-distal isomer (Fig. S25 and S29). Ring currents through the porphyrin macrocycle result in shielding of protons located near or above the porphyrin centre and deshielding of those in the porphyrin periphery.[40–44] Accordingly, we conclude that the amide proton of the *ortho*-proximal isomer is oriented more towards the porphyrin centre, while the amide proton of the *ortho*-distal isomer is directed away from the centre. The amide protons in the two *meta* isomers have similar chemical shifts (10.84 ppm and 10.79 ppm, Fig. S36 and S39), supporting the idea that the chemical shift difference between the two *ortho* isomers truly reflects positional changes rather than different through-bond effects. Furthermore, Nuclear Overhauser Effect Spectroscopy (NOESY) experiments show a cross peak indicating a through-space interaction between the amide proton and one of the peripheral β-pyrrolic protons for the *ortho*-distal isomer (Fig. S30). This finding confirms a predominant conformation wherein the amide proton is oriented away from the porphyrin active site. No such cross peak interactions are seen with the *ortho*-proximal isomer (Fig. S26), indicating that the amide pendant is more rigidly positioned above the porphyrin centre. In sum, the ^{1}H NMR spectra and NOESY data both support the structural conclusions from computational analysis.

2.3 Electrochemical and pK_a measurements under an inert atmosphere

To evaluate the electrochemical behaviour of each isomer in the absence of substrate, cyclic voltammetry (CV) experiments were performed under 1 atm Argon (Ar) in MeCN with 0.1 M tetrabutylammonium hexafluorophosphate ($TBAPF_6$) as supporting electrolyte. Each complex displays three redox events that are typical of iron porphyrins (Fig. S2): a broad $Fe^{III/II}$ couple, which is associated with axial chloride and solvent binding equilibria, and two further reductions that are formally termed $Fe^{II/I}$ and $Fe^{I/0}$, although they are more accurately described as ligand-centred reductions that give the Fe(II) porphyrin radical anion and dianion, respectively.[45,46] The formal $Fe^{I/0}$ couple is most relevant for CO_2 reduction, since the Fe^0 species is traditionally catalytically active.[47–49] At a scan rate of 0.1 V s^{-1}, **Fe-*ortho*-proximal**, **Fe-*meta*-proximal**, and **Fe-*meta*-distal** each display a chemically reversible $Fe^{I/0}$ couple; however, **Fe-*ortho*-distal** only displays a reversible couple at higher scan rates (≥10 V s^{-1}) (Fig. S3). The reduction potentials of the $Fe^{I/0}$ couple ($E_{1/2}(Fe^{I/0})$) for the two *ortho* isomers are ~65 mV more positive than the $E_{1/2}(Fe^{I/0})$ values for the corresponding *meta* isomers (Table 1), and each catalyst is freely diffusing under the specified electrochemical conditions (Fig. S4).

The pK_as of both *ortho* isomers were measured by UV-Vis spectrophotometry in MeCN to determine how distal *versus* proximal positioning of the NH donor might affect amide acidity. These experiments involve equilibration between a deprotonated colorimetric indicator of known pK_a (phenol red) and an amide-functionalized iron porphyrin of unknown pK_a (Fig. S5). As shown in Table 1, **Fe-*ortho*-proximal** (pK_a = 24.7 ± 0.2) and **Fe-*ortho*-distal** (pK_a = 24.1 ± 0.1) have similar pK_as, suggesting that NH donor placement has a relatively minor effect on SCS acidity.

Table 1 Summary of thermodynamic parameters for each amide functionalized Fe-porphyrin

Catalyst	$E_{1/2}(Fe^{I/0})$ (V *vs.* Fc/Fc$^+$)[a]	SCS pK_a (MeCN)[b]
Fe-*ortho*-proximal	−2.000	24.7 ± 0.2
Fe-*ortho*-distal	−1.995	24.1 ± 0.1
Fe-*meta*-proximal	−2.068	—
Fe-*meta*-distal	−2.056	—

[a] Uncertainty is ±5 mV. [b] Values are an average of four separate titration points.

2.4 Electrocatalytic CO_2 reduction in the presence of a mild Brønsted acid

To first assess catalytic activity in the presence of a mild Brønsted acid, we evaluated the electrochemical behaviour of each isomer by CV under 1 atm CO_2 with 50 mM exogenous phenol (pK_a = 29.2 in MeCN).[34] Catalyst concentrations are kept low (0.25 mM) to minimize the effects of catalyst aggregation.[50] Peak-shaped current responses with large i/i_p^0 values (catalytic current normalized to the current in absence of substrate) are observed at potentials near the $Fe^{I/0}$ couple in all cases (Fig. 2 and S6). Notably, **Fe-*ortho*-distal** exhibits a peak i/i_p^0 that is ~5 times lower than the values observed for the other three isomers, suggesting that this catalyst is less active under the specified conditions (*vide infra*). Qualitatively, these data indicate that each isomer is active towards electrocatalytic CO_2 reduction and that catalytic activity depends on positioning of the amide pendant.

Controlled potential electrolysis (CPE) and headspace gas chromatography analysis were performed to evaluate product selectivity across the isomer series. Accordingly, each catalyst was electrolyzed at a potential near the $Fe^{I/0}$ couple under 1 atm CO_2 in the presence of 250 mM phenol (Fig. S8–S11 and Table S1). Under these conditions, three of the four isomers—**Fe-*ortho*-proximal**, **Fe-*meta*-distal**, and **Fe-*meta*-proximal**—display selectivity that is typical for FeTPP catalysts in the presence of

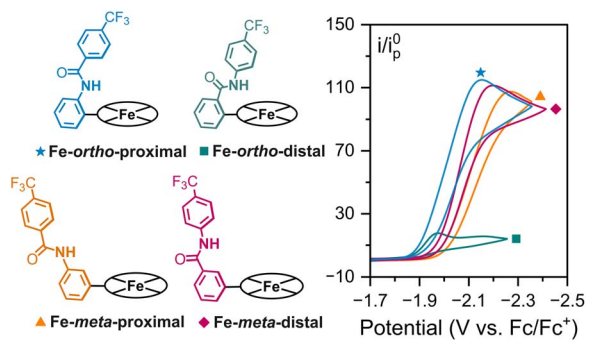

Fig. 2 Catalytic cyclic voltammograms for each iron porphyrin isomer using phenol as the proton donor. Colours and symbols correspond to abbreviated structures shown on the left. Conditions: 0.25 mM catalyst, 50 mM phenol, 1 atm CO_2 (0.28 M), and 0.1 M $TBAPF_6$ in MeCN.

a mild Brønsted acid:[6,13,17,19,47,51,52] $FE_{CO} \geq 80\%$ and $FE_{H_2} \leq 5\%$ (Table 2). By comparison, **Fe-*ortho*-distal** shows somewhat poorer selectivity towards CO ($FE_{CO} = 67 \pm 2\%$) and increased H_2 evolution ($FE_{H_2} = 13 \pm 1\%$), confirming that placement of the NH donor at the *ortho*-distal position adversely alters reaction selectivity. In the presence of a mild exogenous acid, SCS donor positioning therefore appears to have a modest effect on product selectivity.

After evaluating reaction selectivity, we determined how the kinetics of CO_2 reduction depend on NH donor positioning. Kinetics may be extracted from CV data *via* catalytic plateau currents—when side phenomena like substrate consumption or catalyst deactivation are minimal—or by the more general foot-of-the-wave analysis (FOWA), which has been extensively described by Savéant and co-workers.[53,54] At slower scan rates ($0.1\ V\ s^{-1}$) with 50 mM phenol and 1 atm CO_2, plateau currents are not observed (Fig. 2). FOWA was therefore used to extract pseudo-first order rate constants (k_{obs}, s^{-1}) for each catalyst (Table 2 and Fig. S15). At fast scan rates (50 to 250 $V\ s^{-1}$), catalytic plateau currents are obtained for three of the four isomers (**Fe-*ortho*-proximal**, **Fe-*ortho*-distal**, and **Fe-*meta*-distal**) (Fig. S16–S18). The associated k_{obs} values from plateau currents are in good agreement with the kinetics obtained from FOWA, which corroborates the FOWA approach. **Fe-*ortho*-proximal** is the most active catalyst in the series, displaying a k_{obs} that is roughly an order of magnitude larger than the values associated with each of the remaining three isomers. While this comparison does not account for differences in catalyst electronics—wherein a more negative $E_{1/2}(Fe^{I/0})$ often correlates with faster turnover[5,6,17]—**Fe-*ortho*-proximal** displays the largest k_{obs} despite its relatively positive $E_{1/2}(Fe^{I/0})$, which suggests that the SCS in this catalyst engages in significant through-space interactions. It is worth noting that **Fe-*ortho*-distal** displays comparable rate constants to the *meta* isomers despite its significantly lower catalytic peak current (i/i_p^0). This observation may indicate that catalyst inhibition limits the peak current for **Fe-*ortho*-distal** during successive turnovers, as detailed by Savéant.[53,54] We additionally measure a kinetic isotope effect (KIE; H/D) of 1.5–1.7 across the series, confirming that proton transfer contributes to the rate-limiting step of catalysis (Fig. S19 and Table S4). These KIE values are also consistent with previously reported values for FeTPP catalysed CO_2 reduction.[17,30] Together, these results confirm that—under mildly acidic conditions—SCS donor positioning can significantly alter kinetic barriers but leads to only modest changes in reaction selectivity during FeTPP-catalysed CO_2 reduction.

2.5 Electrocatalytic activity and selectivity with a strongly acidic exogenous proton donor

Building on the results with the mild Brønsted acid phenol, we next sought to investigate reaction selectivity and activity with the significantly more acidic 3,5-bis(trifluoromethyl) phenol ($pK_a = 23.8$ in MeCN).[34] With increasing concentrations of acid under 1 atm CO_2, the voltammograms of each catalyst display increasingly large current responses near the $Fe^{I/0}$ couple, consistent with a proton-dependent electrocatalytic response (Fig. 3). It is notable that at lower acid concentrations, **Fe-*ortho*-proximal** exhibits two multi-electron waves—one with peak i/i_p^0 at *ca.* −2.0 V and the second at *ca.* −2.2 V—that become indistinguishable at higher acid concentrations (≥50 mM). This suggests that two separate potential-dependent pathways may

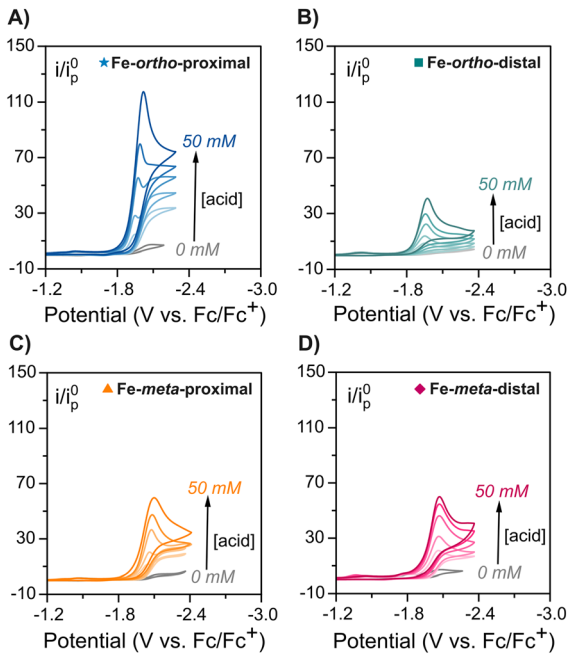

Fig. 3 Catalytic cyclic voltammograms for (A) **Fe-*ortho*-proximal**, (B) **Fe-*ortho*-distal**, (C) **Fe-*meta*-proximal**, and (D) **Fe-*meta*-distal** with increasing amounts of 3,5-bis(trifluoromethyl) phenol. Conditions: 0.25 mM catalyst, 0, 5, 10, 20, 30, and 50 mM 3,5-bis(trifluoromethyl) phenol, 1 atm CO_2 (0.28 M), and 0.1 M $TBAPF_6$ in MeCN.

Table 2 CO_2 reduction selectivity and activity data for each amide positional isomer using phenol as the exogenous acid

Catalyst	FE_{CO}[a] (%)	FE_{H_2}[a] (%)	$\log(k_{obs}/s^{-1})$ (FOWA)[b]	$\log(k_{obs}/s^{-1})$ (plateau)[c]
Fe-*ortho*-proximal	85 ± 3	4 ± 1	4.85 ± 0.06	5.1
Fe-*ortho*-distal	67 ± 2	13 ± 1	3.99 ± 0.08	4.0
Fe-*meta*-proximal	82 ± 1	3 ± 1	3.86 ± 0.07	—
Fe-*meta*-distal	80 ± 1	5 ± 1	4.13 ± 0.08	4.1

[a] Faradaic efficiencies are averages of two independent experiments with [phenol] = 250 mM. [b] Values are averages of 3 independent measurements; uncertainties represent one standard deviation. [c] Uncertainties are estimated at approximately ±15%.[12] All kinetic data were obtained with [phenol] = 50 mM.

be operative with this combination of acid and catalyst. In contrast, the remaining three isomers show only one apparent catalytic wave, even at lower acid concentrations. Compared to their responses with the less acidic phenol, each isomer generally shows a more positive current onset with the stronger acid, which is consistent with faster catalysis and/or involvement of new reaction mechanisms.

To evaluate whether and how product selectivity changes under these more acidic conditions, CPE experiments were performed with each catalyst under 1 atm CO_2 using 50 mM 3,5-bis(trifluoromethyl) phenol (Fig. S12 and Table S2). When **Fe-*ortho*-distal** is electrolysed at potentials near $E_{1/2}(Fe^{I/0})$, minimal quantities of CO are produced ($FE_{CO} = 11 \pm 1\%$) and significant background proton reduction is observed ($FE_{H_2} = 65 \pm 2\%$) (Fig. 4 and Table 3). Both **Fe-*meta*-distal** and **Fe-*meta*-proximal** display similarly unfavourable reaction selectivity. Nevertheless, these three catalysts still show more favourable selectivity than iron tetraphenylporphyrin triflate, **[FeTPP]OTf** (a catalyst lacking amide pendants), which almost exclusively catalyses background proton reduction ($FE_{H_2} = 78 \pm 5\%$) (Fig. S7 and S13, Table 3). This finding suggests that the amide pendants in the three aforementioned isomers still confer a marginal selectivity advantage under the specified acidic conditions. In stark contrast, **Fe-*ortho*-proximal** displays a remarkably high $FE_{CO} = 83 \pm 4\%$ and minimal H_2 evolution ($FE_{H_2} = 7 \pm 1\%$), irrespective of whether the electrolysis is performed near the more positive (*ca.* −2.0 V) or negative (*ca.* −2.2 V) voltammetric feature. These results indicate that the two catalytic waves are associated with two distinct pathways for CO evolution. It is noteworthy that the ratio of CO : H_2 formed with **Fe-*ortho*-proximal** is nearly identical to that obtained under far less acidic conditions (Table 2). Thus, suitably positioned SCS donors prevent indiscriminate proton transfers that otherwise lead to high FE_{H_2} and/or to a lowered total FE for gaseous products (Scheme 3).

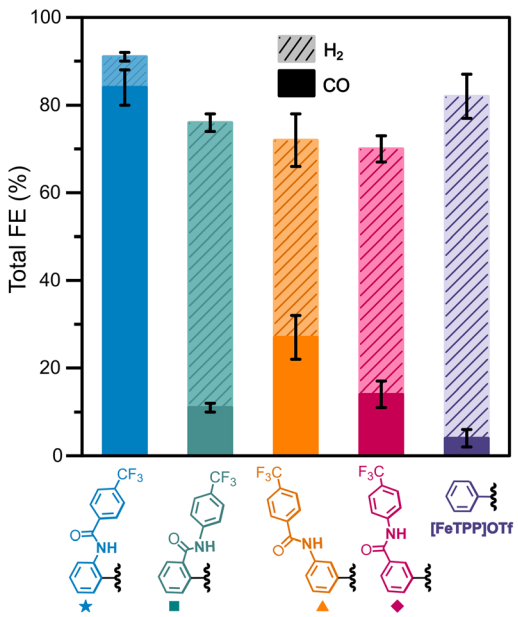

Fig. 4 Faradaic efficiencies (FE) for CO (solid colours) and H_2 (hashed colours) obtained from CPE experiments with each iron porphyrin catalyst in the presence of 3,5-bis(trifluoromethyl) phenol. The amide pendants associated with each iron porphyrin catalyst are depicted beneath the plot, alongside **[FeTPP]OTf** as a control lacking a protic SCS. Conditions: 0.1 mM catalyst, 50 mM 3,5-bis(trifluoromethyl) phenol, 1 atm CO_2, and 0.1 M $TBAPF_6$ in MeCN.

Table 3 CO_2 reduction selectivity and activity data for each iron porphyrin catalyst with 50 mM 3,5-bis(trifluoromethyl) phenol

Catalyst	FE_{CO}[a] (%)	FE_{H_2}[a] (%)	$\log(k_{obs}/s^{-1})$ (plateau)[b]
Fe-*ortho*-proximal	83 ± 4	7 ± 1	4.7
Fe-*ortho*-distal	11 ± 1	65 ± 2	—
Fe-*meta*-proximal	27 ± 5	45 ± 6	—
Fe-*meta*-distal	14 ± 3	55 ± 3	—
[FeTPP]OTf	4 ± 2	78 ± 5	—

[a] Faradaic efficiencies for CO (left) and H_2 (right) that are averages from three independent experiments. [b] Uncertainty is estimated at approximately ±15%.

The favorable selectivity displayed by **Fe-*ortho*-proximal** with 3,5-bis(trifluoromethyl) phenol prompted us to establish a practical limit to exogenous acid acidity. Accordingly, we evaluated the CO_2 reduction selectivity of **Fe-*ortho*-proximal** in the presence of 50 mM pentafluorophenol ($pK_a = 20.1$)[34] (Fig. S14). When this catalyst is electrolyzed at potentials near $E_{1/2}(Fe^{I/0})$ under 1 atm of CO_2, minimal quantities of CO are observed ($FE_{CO} = 7 \pm 1\%$), and H_2 is obtained as the major reduction product ($FE_{H_2} = 66 \pm 2\%$) (Table S3). Thus, the pK_a of 3,5-bis(trifluoromethyl) phenol likely represents the maximum acidity limit wherein **Fe-*ortho*-proximal** remains selective towards CO, and further decreasing the exogenous acid pK_a by ~4 units results in poor reaction selectivity.

After evaluating the selectivity of each catalyst, we next sought to measure catalytic rate constants under these strongly acidic conditions and compare them to the kinetic parameters

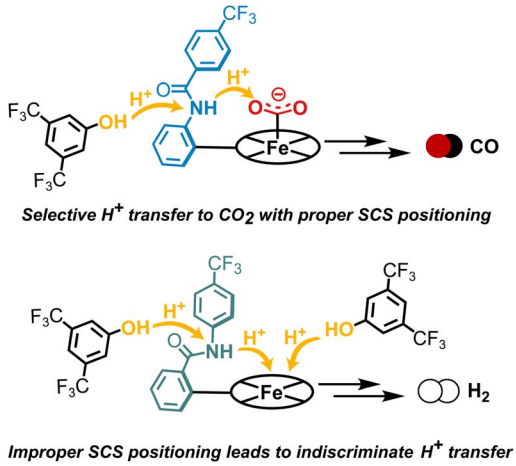

Scheme 3 Simplified reaction scheme showing how suitably positioned SCS groups promote selective CO_2 reduction (top), while improperly positioned SCS donors enable indiscriminate proton transfers that lead to H_2 and an overall decrease in total FE for gaseous products (bottom).

obtained in the presence of phenol. This analysis was restricted to **Fe-*ortho*-proximal** with 3,5-bis(trifluoromethyl) phenol, as it is the only isomer/acid pairing with high selectivity for CO and thus the only catalyst for which the current response is mostly attributable to a single reaction product. The presence of two overlapping catalytic features when using 3,5-bis(trifluoromethyl) phenol precludes reliable application of FOWA to determine k_{obs}. Instead, we report a k_{obs} that is derived from catalytic plateau currents at high scan rates (100 V s^{-1}) and note that this value likely represents an amalgamation of the rate constants associated with the two operating catalytic pathways (Fig. S20). The log(k_{obs}) of 4.7 measured with 3,5-bis(trifluoromethyl) phenol (Table 3) is similar to the log(k_{obs}) of 5.1 obtained with phenol (Table 2).

This similarity in k_{obs} is initially surprising, as it contrasts with previous work from our group demonstrating that more acidic exogenous phenols can significantly increase CO_2 reduction rate constants.[18] Savéant and co-workers have also reported a similar Brønsted relationship with unfunctionalized FeTPP and a range of structurally diverse exogenous acids.[30] Departure from the expected Brønsted relationship could arise if k_{obs} has contributions from multiple catalytic pathways or if there is a substantial change in the character of the rate-limiting transition state under highly acidic conditions. Another possible explanation is that the similar k_{obs} values obtained with different exogenous acids is due to the SCS amide's role as a proton relay in the rate-limiting step of catalysis. Once the exogenous acid is sufficiently acidic and present in high enough concentration to favour fast SCS re-protonation, k_{obs} should depend only on the intramolecular proton transfer step and therefore should become invariant with exogenous acid concentration.[55,56] Indeed, we find that k_{obs} becomes independent of 3,5-bis(trifluoromethyl) phenol concentration at acid concentrations >50 mM (Fig. S21).

Since water can play a key role in SCS proton transfers,[21,23,24,29,57] we investigated the potential role of adventitious water on catalytic activity. We thereby measured kinetic parameters with dry MeCN electrolyte and 3,5-bis(trifluoromethyl) phenol at a concentration where catalytic rates still depend on exogenous acid concentration (20 mM) in the presence of an equimolar concentration of water (Fig. S22). Under these conditions, the value of log(k_{obs}) is 4.1 and does not significantly change in the presence or absence of water, confirming that adventitious water plays a minimal role during rate-limiting proton transfer.

The electrocatalytic behaviour of **Fe-*ortho*-proximal** with 3,5-bis(trifluoromethyl) phenol as an exogenous acid is clearly more complex than what is typical for FeTPP catalysts.[30,47,58] Based on computational results and NMR spectroscopy, it appears that the NH donor in **Fe-*ortho*-proximal** is ideally oriented to direct proton transfers from the exogenous acid to bound CO_2 at the active site. In contrast, the lowest energy conformers of the other three catalysts indicate that the NH donors are either too far away (in the case of **Fe-*meta*-proximal** and **Fe-*meta*-distal**) or misdirected (as for **Fe-*ortho*-distal**). We propose that this difference in alignment of the proton transfer coordinate is responsible for the selectivity enhancement observed with **Fe-*ortho*-proximal**. It is also possible that this change in donor positioning results in stronger or weaker hydrogen bonding interactions between the SCS and CO_2, and that more suitably positioned NH donors (*i.e.*, **Fe-*ortho*-proximal**) might better stabilize the catalyst-CO_2 adduct; however, in our previous report describing a series of *ortho*-proximal isomers bearing amides of variable pK_a, we found that these SCS amides have a minimal influence on the CO_2 binding equilibrium,[18] suggesting that the differences in product selectivity described here are more likely the result of an SCS proton relay effect. Furthermore, we speculate that the optimal alignment of an SCS proton donor lowers transition state energies for multiple CO_2 reduction pathways that differ in the sequence of electron and proton transfers. In a related fashion, Aukauloo and co-workers reported an FeTPP catalyst bearing SCS urea groups that activates CO_2 *via* the unconventional formal Fe^{I} oxidation state.[26] The Dempsey group also observed a similar phenomenon during proton reduction, wherein changes to solution and SCS acidity alter the sequence of proton and electron transfer events leading to metal hydride formation.[59–61] Continued exploration of the interplay between SCS donor positioning and solution acidity may thus present opportunities to investigate novel changes in both the reaction mechanism and selectivity of FeTPP-catalysed CO_2 reduction.

3. Conclusions

Herein, we have evaluated the product selectivity of four iron porphyrin isomers bearing a pendent amide at varying positions around the catalytic active site. The NH donor of each amide was installed at the *ortho*- or *meta*-positions of the *meso* porphyrin ring, and either proximal or distal to the iron porphyrin core. In the presence of phenol—a conventionally mild Brønsted acid—each isomer shows favourable selectivity for CO, with minimal H_2 evolution. Under these conditions, the **Fe-*ortho*-proximal** isomer displays the most favourable kinetics, confirming that suitable positioning of SCS groups can lower the barrier to CO_2 reduction. Remarkably, in the presence of a significantly more acidic exogenous acid—3,5-bis(trifluoromethyl) phenol—it is found that SCS donor positioning has a significant effect on reaction selectivity: **Fe-*ortho*-proximal** remains highly selective for CO, while the remaining three isomers mainly promote undesired H_2 evolution. Together, these results demonstrate that proper SCS donor positioning is an important design consideration that can beneficially alter reaction selectivity, particularly with regard to avoiding indiscriminate proton transfers. This work motivates future investigations into the role of SCS donor positioning on changing reaction outcomes, and how such effects might be relevant to promoting the ever-challenging reduction of CO_2 beyond $2e^-$.

Author contributions

KT and EMN conceived of the project and wrote the manuscript, while JPR performed all computational analysis. KT conducted all other experimental work and data analysis.

Conflicts of interest

There are no conflicts to declare.

Data availability

The data supporting this article have been included as part of the SI. Supplementary information: experimental procedures, characterization data, and computational details. See DOI: https://doi.org/10.1039/d5sc04700e.

Acknowledgements

This work was supported by the University of British Columbia, the Natural Sciences and Engineering Research Council of Canada (RGPIN-2021-03691 and DGECR-2021-00427), and the Research Corporation for Science Advancement (27752). KT acknowledges support from a British Columbia Graduate Fellowship as well as UBC Chemistry for a Head's departmental scholarship. EMN is grateful to CIFAR for support as an Azrieli Global Scholar. Computational resources were provided from the Digital Research Alliance of Canada and the Advanced Research Computing (ARC) centre at the University of British Columbia.

Notes and references

1 A. M. Appel, J. E. Bercaw, A. B. Bocarsly, H. Dobbek, D. L. DuBois, M. Dupuis, J. G. Ferry, E. Fujita, R. Hille, P. J. A. Kenis, C. A. Kerfeld, R. H. Morris, C. H. F. Peden, A. R. Portis, S. W. Ragsdale, T. B. Rauchfuss, J. N. H. Reek, L. C. Seefeldt, R. K. Thauer and G. L. Waldrop, *Chem. Rev.*, 2013, **113**, 6621–6658.
2 O. S. Bushuyev, P. De Luna, C. T. Dinh, L. Tao, G. Saur, J. van de Lagemaat, S. O. Kelley and E. H. Sargent, *Joule*, 2018, **2**, 825–832.
3 A. J. Morris, G. J. Meyer and E. Fujita, *Acc. Chem. Res.*, 2009, **42**, 1983–1994.
4 E. E. Benson, C. P. Kubiak, A. J. Sathrum and J. M. Smieja, *Chem. Soc. Rev.*, 2009, **38**, 89–99.
5 I. Azcarate, C. Costentin, M. Robert and J.-M. Savéant, *J. Phys. Chem. C*, 2016, **120**, 28951–28960.
6 I. Azcarate, C. Costentin, M. Robert and J.-M. Savéant, *J. Am. Chem. Soc.*, 2016, **138**, 16639–16644.
7 C. L. Drennan, J. Heo, M. D. Sintchak, E. Schreiter and P. W. Ludden, *Proc. Natl. Acad. Sci. U. S. A.*, 2001, **98**, 11973–11978.
8 W. W. Cleland, T. J. Andrews, S. Gutteridge, F. C. Hartman and G. H. Lorimer, *Chem. Rev.*, 1998, **98**, 549–562.
9 M. Zhao, H.-B. Wang, L.-N. Ji and Z.-W. Mao, *Chem. Soc. Rev.*, 2013, **42**, 8360–8375.
10 M. W. Drover, *Chem. Soc. Rev.*, 2022, **51**, 1861–1880.
11 J. Trouvé and R. Gramage-Doria, *Chem. Soc. Rev.*, 2021, **50**, 3565–3584.
12 D. J. Martin and J. M. Mayer, *J. Am. Chem. Soc.*, 2021, **143**, 11423–11434.
13 A. Chapovetsky, M. Welborn, J. M. Luna, R. Haiges, T. F. Miller III and S. C. Marinescu, *ACS Cent. Sci.*, 2018, **4**, 397–404.
14 A. W. Nichols and C. W. Machan, *Front. Chem.*, 2019, **7**, 1–19.
15 C. Costentin, S. Drouet, M. Robert and J.-M. Savéant, *Science*, 2012, **338**, 90–94.
16 C. Costentin, G. Passard, M. Robert and J.-M. Savéant, *J. Am. Chem. Soc.*, 2014, **136**, 11821–11829.
17 E. M. Nichols, J. S. Derrick, S. K. Nistanaki, P. T. Smith and C. J. Chang, *Chem. Sci.*, 2018, **9**, 2952–2960.
18 K. Teindl, B. O. Patrick and E. M. Nichols, *J. Am. Chem. Soc.*, 2023, **145**, 17176–17186.
19 C. G. Margarit, C. Schnedermann, N. G. Asimow and D. G. Nocera, *Organometallics*, 2019, **38**, 1219–1223.
20 C. G. Margarit, N. G. Asimow, M. I. Gonzalez and D. G. Nocera, *J. Phys. Chem. Lett.*, 2020, **11**, 1890–1895.
21 P. Sen, B. Mondal, D. Saha, A. Rana and A. Dey, *Dalton Trans.*, 2019, **48**, 5965–5977.
22 A. Sonea, N. R. Crudo and J. J. Warren, *J. Am. Chem. Soc.*, 2024, **146**, 3721–3731.
23 J. S. Derrick, M. Loipersberger, S. K. Nistanaki, A. V. Rothweiler, M. Head-Gordon, E. M. Nichols and C. J. Chang, *J. Am. Chem. Soc.*, 2022, **144**, 11656–11663.
24 P. Gotico, B. Boitrel, R. Guillot, M. Sircoglou, A. Quaranta, Z. Halime, W. Leibl and A. Aukauloo, *Angew. Chem., Int. Ed.*, 2019, **58**, 4504–4509.
25 A. Sonea, K. L. Branch and J. J. Warren, *ACS Catal.*, 2023, **13**, 3902–3912.
26 S. Amanullah, P. Gotico, M. Sircoglou, W. Leibl, M. J. Llansola-Portoles, T. Tibiletti, A. Quaranta, Z. Halime and A. Aukauloo, *Angew. Chem., Int. Ed.*, 2024, **63**, e202314439.
27 H. Rao, L. C. Schmidt, J. Bonin and M. Robert, *Nature*, 2017, **548**, 74–77.
28 S. Amanullah, P. Saha and A. Dey, *J. Am. Chem. Soc.*, 2021, **143**, 13579–13592.
29 S. Ghosh, S. Patra, A. Bisoi, S. Ghosh, N. Maurya, A. Das, P. C. Singh and A. Dey, *ACS Catal.*, 2025, **15**, 3595–3610.
30 C. Costentin, S. Drouet, G. Passard, M. Robert and J.-M. Savéant, *J. Am. Chem. Soc.*, 2013, **135**, 9023–9031.
31 C. G. Margarit, N. G. Asimow, C. Costentin and D. G. Nocera, *ACS Energy Lett.*, 2020, **5**, 72–78.
32 I. Bhugun, D. Lexa and J.-M. Savéant, *J. Am. Chem. Soc.*, 1996, **118**, 3982–3983.
33 F. Bordwell and D. Algrim, *J. Org. Chem.*, 1976, **41**, 2507–2508.
34 A. Kütt, S. Tshepelevitsh, J. Saame, M. Lõkov, I. Kaljurand, S. Selberg and I. Leito, *Eur. J. Org Chem.*, 2021, **2021**, 1407–1419.
35 F. G. Bordwell and J. Cheng, *J. Am. Chem. Soc.*, 1991, **113**, 1736–1743.
36 S. S. Roy, K. Talukdar and J. W. Jurss, *ChemSusChem*, 2021, **14**, 662–670.
37 M. L. Pegis, B. A. McKeown, N. Kumar, K. Lang, D. J. Wasylenko, X. P. Zhang, S. Raugei and J. M. Mayer, *ACS Cent. Sci.*, 2016, **2**, 850–856.

38 S. Sinha and J. J. Warren, *Inorg. Chem.*, 2018, **57**, 12650–12656.
39 K. T. Ngo, M. McKinnon, B. Mahanti, R. Narayanan, D. C. Grills, M. Z. Ertem and J. Rochford, *J. Am. Chem. Soc.*, 2017, **139**, 2604–2618.
40 U. Simonis, F. A. Walker, P. L. Lee, B. J. Hanquet, D. J. Meyerhoff and W. R. Scheidt, *J. Am. Chem. Soc.*, 1987, **109**, 2659–2668.
41 J. P. Collman, X. Zhang, K. Wong and J. I. Brauman, *J. Am. Chem. Soc.*, 1994, **116**, 6245–6251.
42 D. Reddy and T. K. Chandrashekar, *J. Chem. Soc., Dalton Trans.*, 1992, 619–625.
43 J. P. Collman, A. O. Chong, G. B. Jameson, R. T. Oakley, E. Rose, E. R. Schmittou and J. A. Ibers, *J. Am. Chem. Soc.*, 1981, **103**, 516–533.
44 C. J. Medforth, in *Fundamentals of Porphyrin Chemistry*, 2022, pp. 611–629.
45 C. Römelt, J. Song, M. Tarrago, J. A. Rees, M. van Gastel, T. Weyhermüller, S. DeBeer, E. Bill, F. Neese and S. Ye, *Inorg. Chem.*, 2017, **56**, 4745–4750.
46 C. Römelt, S. Ye, E. Bill, T. Weyhermüller, M. van Gastel and F. Neese, *Inorg. Chem.*, 2018, **57**, 2141–2148.
47 I. Bhugun, D. Lexa and J.-M. Savéant, *J. Am. Chem. Soc.*, 1996, **118**, 1769–1776.
48 I. Bhugun, D. Lexa and J.-M. Savéant, *J. Phys. Chem.*, 1996, **100**, 19981–19985.
49 M. Hammouche, D. Lexa, J. M. Savéant and M. Momenteau, *J. Electroanal. Chem. Interfacial Electrochem.*, 1988, **249**, 347–351.
50 K. L. Branch, E. R. Johnson and E. M. Nichols, *ACS Cent. Sci.*, 2024, **10**, 1251–1261.
51 K. Kosugi, M. Kondo and S. Masaoka, *Angew. Chem., Int. Ed.*, 2021, **60**, 22070–22074.
52 M. R. Narouz, P. De La Torre, L. An and C. J. Chang, *Angew. Chem., Int. Ed.*, 2022, **61**, e202207666.
53 C. Costentin, S. Drouet, M. Robert and J.-M. Savéant, *J. Am. Chem. Soc.*, 2012, **134**, 11235–11242.
54 C. Costentin and J.-M. Savéant, *ChemElectroChem*, 2014, **1**, 1226–1236.
55 M. Haake, B. Reuillard, M. Chavarot-Kerlidou, C. Costentin and V. Artero, *Angew. Chem., Int. Ed.*, 2024, **63**, e202413910.
56 J.-M. Savéant, *Angew. Chem., Int. Ed.*, 2019, **58**, 2125–2128.
57 C.-Y. Yeh, C. J. Chang and D. G. Nocera, *J. Am. Chem. Soc.*, 2001, **123**, 1513–1514.
58 C. Costentin, M. Robert and J.-M. Savéant, *Chem. Soc. Rev.*, 2013, **42**, 2423–2436.
59 C. L. Montgomery, M. Z. Ertem, L. Chevalier and J. L. Dempsey, *J. Am. Chem. Soc.*, 2024, **146**, 30020–30032.
60 C. L. Montgomery, M. Z. Ertem, Z. H. Claytor and J. L. Dempsey, *Inorg. Chem.*, 2025, **64**, 10139–10149.
61 C. L. Montgomery, J. Amtawong, A. M. Jordan, D. A. Kurtz and J. L. Dempsey, *Chem. Soc. Rev.*, 2023, **52**, 7137–7169.